



## Observations of Kelvin-Helmholtz waves along the dusk-side boundary of Mercury's magnetosphere during MESSENGER's third flyby

Scott A. Boardsen,<sup>1,2</sup> Torbjörn Sundberg,<sup>3</sup> James A. Slavin,<sup>1</sup> Brian J. Anderson,<sup>4</sup> Haje Korth,<sup>4</sup> Sean C. Solomon,<sup>5</sup> and Lars G. Blomberg<sup>3</sup>

Received 13 April 2010; revised 29 April 2010; accepted 3 May 2010; published 18 June 2010.

[1] During the third MESSENGER flyby of Mercury on 29 September 2009, 15 crossings of the dusk-side magnetopause were observed in the magnetic field data over a 2-min period, during which the spacecraft traveled a distance of  $0.2 R_M$  (where  $R_M$  is Mercury's radius). The quasi-periodic nature of the magnetic field variations during the crossings, the characteristic time separations of  $\sim 16$  s between pairs of crossings, and the variations of the magnetopause normal directions indicate that the signals are likely the signature of surface waves highly steepened at their leading edge that arose from the Kelvin-Helmholtz instability. At Earth, the Kelvin-Helmholtz instability is believed to lead to the turbulent transport of solar wind plasma into Earth's plasma sheet. This solar wind entry mechanism could also be important at Mercury. **Citation:** Boardsen, S. A., T. Sundberg, J. A. Slavin, B. J. Anderson, H. Korth, S. C. Solomon, and L. G. Blomberg (2010), Observations of Kelvin-Helmholtz waves along the dusk-side boundary of Mercury's magnetosphere during MESSENGER's third flyby, *Geophys. Res. Lett.*, *37*, L12101, doi:10.1029/2010GL043606.

### 1. Introduction

[2] Kelvin-Helmholtz (K-H) waves driven by solar wind flow around planetary magnetospheres have been reported at Earth [e.g., *Fairfield et al.*, 2000; *Hasegawa et al.*, 2004, 2009] and Saturn [*Masters et al.*, 2009, 2010], most convincingly by the identification of vortices at both bodies [*Hasegawa et al.*, 2004; *Masters et al.*, 2010]. Mercury's close proximity to the Sun offers the opportunity to observe these waves under much higher solar wind pressure, higher interplanetary magnetic field (IMF) intensities, and lower Alfvénic Mach numbers than those typically observed at 1 AU or in the outer solar system. Further, the small size of this magnetosphere relative to the Larmor radii of shocked solar wind and planetary ions is important. Typically at

Earth the thickness of the magnetopause current layer is many ( $\sim 10$ ) times the magnetosheath ion Larmor radii [*Berchem and Russell*, 1982], so the effects of finite Larmor radius are difficult to observe. Kinetic simulations [*Wilber and Winglee*, 1995; *Nakamura et al.*, 2010] show that, as the velocity-shear layer thickness approaches the ion Larmor diameter, strong dawn/dusk asymmetries arise. Because Mercury's magnetosphere is  $\sim 8$  times smaller than Earth's magnetosphere, finite ion Larmor-radius effects at Mercury should be more readily observable. Moreover, because Mercury does not have an ionosphere, there is no ionospheric dissipation of these waves as they propagate down the magnetospheric flanks, in contrast to the situation at Earth where such dissipation is strong [e.g., *Lemaire*, 1977].

[3] *Slavin et al.* [2008, 2009] reported the observation of three azimuthal rotations in the magnetic field direction near Mercury's magnetopause during the first flyby (M1) by the MERcury Surface, Space ENvironment, GEochemistry, and Ranging (MESSENGER) spacecraft on 14 January 2008. The IMF direction was northward and was therefore favorable to the development of K-H waves in the magnetosphere. From a detailed analysis of this event, T. Sundberg et al. (The Kelvin-Helmholtz instability at Mercury: An assessment, submitted to *Planetary and Space Science*, 2010) concluded that the wave signature was not that of a nonlinear K-H wave and that the magnetopause showed no signs of any perturbations. The period of these rotations was  $\sim 70$  s, and the wavelength was estimated to be  $\sim 4$ – $10 R_M$ , where  $R_M$  is Mercury's radius. Determination of magnetic field orientations near the magnetopause is important because magnetic tension forces in the flow direction tend to stabilize this boundary. During M1 the tailward component of the magnetic field was small on the magnetosheath side and was dominant on the magnetospheric side of the magnetopause.

[4] No evidence of K-H waves was detected during the second MESSENGER flyby of Mercury (M2) on 6 October 2008, during which the IMF component normal to Mercury's orbital plane was strongly southward. During M2, the magnetic tension arising from the large tailward magnetic field component ( $\sim 30$  nT) observed on both sides of the magnetopause acted to suppress the K-H instability.

[5] During MESSENGER's third Mercury flyby (M3) on 29 September 2009, multiple magnetopause crossings were observed by the MESSENGER Magnetometer along the (inbound) dusk-side leg of the trajectory, and *Slavin et al.* [2010] suggested that the multiple crossings could be due to the K-H instability. Here we present an analysis of these boundary encounters, and we compare the results with the predictions of theory. Our findings indicate that

<sup>1</sup>Heliophysics Science Division, NASA Goddard Space Flight Center, Greenbelt, Maryland, USA.

<sup>2</sup>Goddard Earth Sciences and Technology Center, University of Maryland, Baltimore County, Baltimore, Maryland, USA.

<sup>3</sup>Space and Plasma Physics, School of Electrical Engineering, Royal Institute of Technology, Stockholm, Sweden.

<sup>4</sup>Johns Hopkins University Applied Physics Laboratory, Laurel, Maryland, USA.

<sup>5</sup>Department of Terrestrial Magnetism, Carnegie Institution of Washington, Washington, D. C., USA.

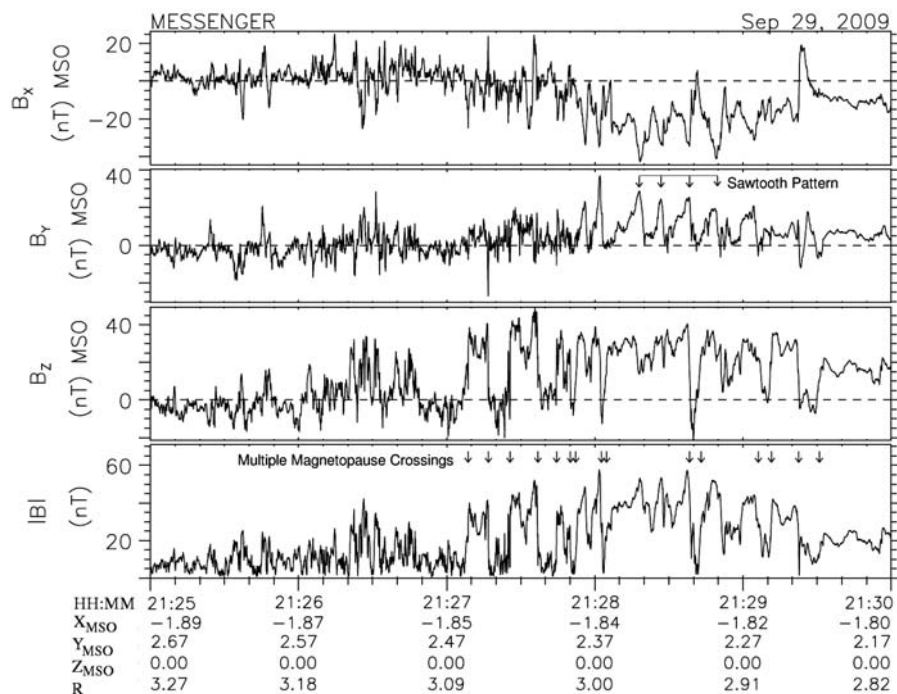


**Figure 1.** Time series of (top to bottom) the  $X$ ,  $Y$ , and  $Z$  components of the magnetic field and the field magnitude during MESSENGER's inbound encounter with Mercury's magnetopause on 29 September 2009. As MESSENGER moved from the magnetosheath into the magnetosphere it encountered multiple crossings of the magnetopause [indicated by arrows in Figure 1 (bottom)].

MESSENGER may have observed highly steepened, possibly turbulent, K-H boundary waves during its third flyby crossing of the dusk-side boundary of Mercury's magnetosphere.

## 2. Observations

[6] We use MESSENGER Magnetometer [Anderson *et al.*, 2007] data at a sampling rate of  $20 \text{ s}^{-1}$  for this study. The M3 trajectory was close to Mercury's equatorial plane, and the spacecraft traversed from the dusk to the dawn side. The average inbound IMF components ( $B_X$ ,  $B_Y$ ,  $B_Z$ ) were  $\sim(-27.8, 4.6, -0.3)$  nT just before the bow-shock crossing at  $\sim 20:27:57$  UTC, where  $X$ ,  $Y$ , and  $Z$  are in Mercury solar orbital (MSO) coordinates. (In these coordinates  $X$  is directed from the center of the planet toward the Sun,  $Z$  is normal to Mercury's orbital plane and positive toward the north celestial pole, and  $Y$  completes the right-handed coordinate system.) The shocked IMF during the first half of the magnetosheath crossing, averaging  $\sim(-41.3, 17.9, 5.3)$  nT, was similar to that in the solar wind. In contrast, during the second half of the magnetosheath crossing, the shocked IMF, averaging  $\sim(-1.4, -2.5, -1.9)$  nT, was very different and displayed a substantial reduction in magnitude of the  $B_X$  and  $B_Y$  components. The shocked IMF  $B_Z$  component changed sign multiple times in the magnetosheath and was primarily positive during the first half of the crossing and primarily negative ( $\sim 75\%$  of the time) during the second half. Between the first and second magnetopause crossings, the magnetospheric magnetic field was  $\sim(-6.8, 5.8, 34.5)$  nT. During M3 the tailward component was not dominant either in the magnetosheath or on the magnetospheric side of the magnetopause.

[7] Time series plots of Magnetometer measurements for the dusk-side (inbound) transition from the magnetosheath to the magnetosphere are shown in Figure 1. Fifteen magnetopause crossings between 21:27:09 and 21:29:31 UTC, eight from the magnetosheath to the magnetosphere and seven from the magnetosphere to the magnetosheath, are indicated by arrows. Because the IMF  $B_Z$  was primarily negative during the second half of the magnetosheath passage, the criterion used for detecting a magnetopause crossing was a sign transition in  $B_Z$  coupled with a strong change in the magnitude of  $B$ . Brief encounters with the magnetopause probably also occurred from 21:25:20 to 21:26:48 UTC. Note the increase and subsequent decrease in the envelope formed by the peak field magnitudes from this set of 15 crossings and spread over a  $\sim 2$  min interval. This change in envelope strength is associated with the first of four magnetic flux loading/unloading events in Mercury's magnetotail, spaced at  $\sim 4$  min intervals, discussed by Slavin *et al.* [2010].

[8] These magnetopause crossings were quasi-periodic, with a characteristic time of  $\sim 16$  s between successive magnetosheath-to-magnetosphere crossings. At about 21:28 UTC the spacecraft transitioned from being primarily in the magnetosheath to being primarily in the magnetosphere. After that point both the  $B_X$  and  $B_Y$  components tended to be negative and positive, respectively, and a distinct sawtooth pattern can be seen in  $B_Y$  and to a lesser extent in  $B_X$ . The period of the sawtooth signatures is similar to that of the magnetopause crossings. The extrema in the  $B_Y$  component generally coincide with extrema of opposite polarity in the  $B_X$  component, a result consistent with magnetohydrodynamic (MHD) simulations [Otto and Fairfield, 2000] of terrestrial K-H waves observed by the Geotail spacecraft [Fairfield *et al.*

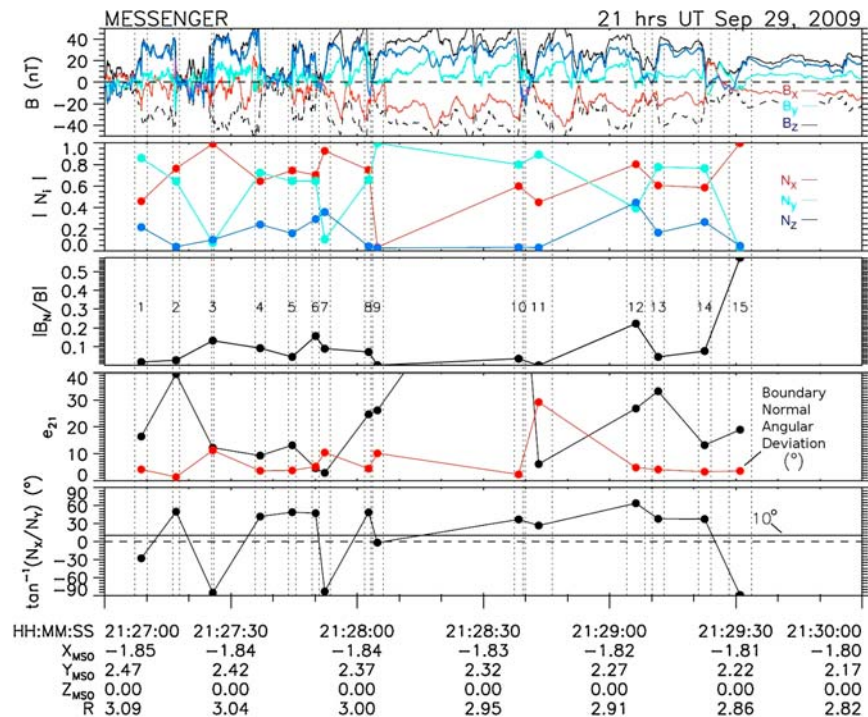


**Figure 2.** Results of minimum variance analysis of the 15 magnetopause crossings shown in Figure 1. Vertical dashed lines indicate each analysis interval. (top panel) Magnetic field magnitude (black) and field components in MSO coordinates. (second panel) Absolute values of the components of the boundary normal in MSO coordinates. (third panel) Absolute values of the ratio of the boundary-normal component of the magnetic field to the total magnetic field. (fourth panel) Ratio of intermediate to minimum eigenvalues and angular standard deviation of each boundary normal. (bottom panel) Boundary-normal angle.

*al.*, 2000]. In those simulations such extrema are associated with K-H vortices in which the field components are compressed as the vortex develops. One difference is that at Mercury  $B_X$  changed sign infrequently over the sawtooth interval, whereas in Geotail observations at Earth  $B_X$  changed sign at each vortex crossing.

[9] Minimum variance analysis (MVA) [Sonnerup and Scheible, 1998] was performed on these magnetopause crossings to determine their boundary normal directions, and the results are shown in Figure 2. The time interval selected for MVA was adjusted in each case to maximize the ratio  $e_{21}$  of intermediate to minimum eigenvalues, to sharpen boundary-normal definition [Sonnerup and Scheible, 1998], while maintaining a large change in field magnitude across that interval. In general, the magnitude of the  $Z$  component of the boundary normal  $N$  (Figure 2, second panel) tends to be much smaller than those of the  $X$  and  $Y$  components and is never the dominant component, an outcome expected by the fact that the spacecraft trajectory was nearly in the MSO equatorial plane. The ratio of the boundary normal component ( $B_N$ ) to the field magnitude ( $B$ )  $B_N/B$  was computed from the averages of  $B_N$  and  $B$  over each analysis interval. The magnetopause can be approximated by a tangential discontinuity for crossings in which  $B_N/B$  (Figure 2, third panel) is small, a condition that holds for all crossings except number 15.

[10] The ratios of intermediate to minimum eigenvalue (Figure 2, fourth panel) are all greater than 2.9, and most are greater than 10, lending confidence to our boundary normal estimates. In addition, the angular standard deviation of each

boundary normal was computed from estimates of the normal for eight nested time intervals centered on that used for the nominal calculation, four smaller than and four larger than the nominal interval. Except for one interval (11), the standard deviation is less than  $12^\circ$ . The average boundary-normal angle in the  $X$ - $Y$  plane,  $\tan^{-1}(N_X/N_Y)$ , is  $10^\circ$  (Figure 2, bottom panel), but there is considerable deviation of the boundary normal angles about that average.

[11] Because the boundary normals determined by MVA have a sign ambiguity, the following procedure was used to resolve this ambiguity. On the basis of the quasi-periodicity of the magnetopause crossings, we assume that these crossings sampled surface waves on the magnetopause. We assume further that the waves sampled were quasi-stationary and propagating tailward along the magnetopause at a velocity much greater than the spacecraft velocity of 4.2 km/s in a Mercury-centered frame of reference. Our convention is that the boundary normals point outward from the local magnetopause into the local magnetosheath. This geometry is illustrated in the wave frame of reference in Figure 3a, which shows a smooth (and non-unique) surface drawn through the tangents of the observed wave-normal directions. As the spacecraft crosses the wave surface (red line) from the magnetosheath (magnetosphere) into the magnetosphere (magnetosheath), the parallel component of the boundary normal vector points anti-sunward (sunward). Under this convention and the above assumptions,  $N_X < 0$  inbound from magnetosheath to magnetosphere and  $N_X > 0$  outbound from magnetosphere to magnetosheath. For Figure 3a, the phase velocity ( $V_p$ ) of the wave was assumed

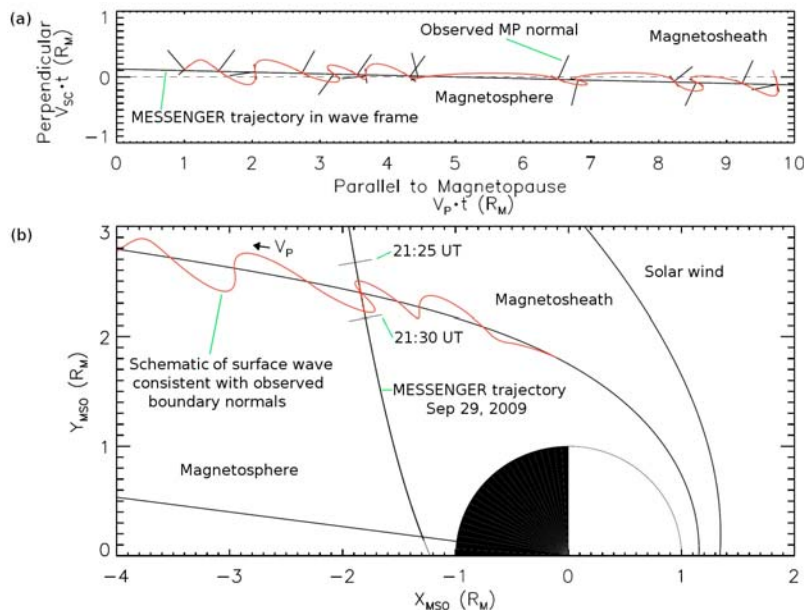


**Figure 3.** (a) Schematic depiction of the magnetopause (MP) surface in the wave frame of reference that is tangent to the observed boundary normals. For crossings from magnetosheath (magnetosphere) to magnetosphere (magnetosheath) the parallel component of the boundary normal points away from (toward) the Sun. The dashed line denotes the average position of the magnetopause. The parallel position is the product of the phase velocity  $V_p$  and time  $t$ , and the perpendicular position is the product of spacecraft velocity  $V_{sc}$  and  $t$ . (b) A schematic view of the observed waves inferred from the first nine magnetopause crossings in a Mercury-fixed frame of reference.

to be 150 km/s, and the magnetopause was rotated  $-12.6^\circ$  ( $8^\circ$  due to aberration plus  $4.6^\circ$  due to flaring of the magnetopause) in the  $X$ - $Y$  plane. The boundary normals indicate that this wave is highly steepened on its leading edge, an observation consistent with steepening at the leading (tailward) edge as documented by the Cluster spacecraft at Earth [Owen *et al.*, 2004], in contrast to steepening of the trailing (sunward) edge as observed by the ISEE 1 and 2 spacecraft at Earth [Chen and Kivelson, 1993]. An illustration of this wave propagating tailward along Mercury’s magnetopause is shown in Figure 3b.

### 3. Discussion

[12] On the basis of similarity to magnetic field measurements of multiple magnetopause crossing intervals along the flanks of Earth’s magnetosphere [e.g., Fairfield *et al.*, 2000], the multiple crossings observed at Mercury during M3 are likely due to the K-H instability. There are nonetheless some differences between the M3 observations and those at Earth [e.g., Fairfield *et al.*, 2000, 2007; Hasegawa *et al.*, 2009]. During M3 the magnetic field maxima occurred within the magnetosphere, rather than within the magnetosheath as at Earth. The IMF was strongly northward for these terrestrial observations, whereas for M3 the magnetosheath  $B_z$  component was predominantly southward. Southward  $B_z$  does not preclude the development of K-H waves, but the compressive MHD linear growth rate for the K-H instability is about a factor of 3 smaller for southward IMF than for northward IMF [Miura, 1995]. The reduction in tailward magnetic tension resulting from the decrease in magnetosheath field strength

shortly before the magnetopause encounters likely created conditions favorable for this instability.

[13] Given the lack of plasma measurements and the limitations posed by only a single observing platform, only crude estimates can be made of the most unstable wavelengths. A magnetosheath flow velocity ( $V_F$ ) of 350 km/s, density of  $64 \text{ cm}^{-3}$ , magnetosonic Mach number ( $M_S$ ) of 2.5, and ion thermal speed ( $V_{thi} = V_F/M_S$ ) of  $\sim 150$  km/s can be estimated from gas dynamic models [Spreiter *et al.*, 1966] and predictions of coupled coronal-heliospheric models [Baker *et al.*, 2009; Odstrcil *et al.*, 2009] at Mercury for a solar wind velocity of 410 km/s and density of  $80 \text{ cm}^{-3}$ . (MESSENGER does not measure properties of the solar wind.) For simplicity, we also assume that the velocity shear across the magnetopause is given by  $\delta V \sim V_F$ . For a  $V_p$  value of  $\sim 175$  km/s ( $0.5 V_F$ ) and a  $\sim 16$ -s period, the wavelength is  $\sim 2800$  km ( $1.1 R_M$ ).

[14] On the basis of full kinetic 2.5-dimensional simulations, Nakamura *et al.* [2010] showed that the boundary layer will rapidly adjust its thickness to a width that is greater than an “effective” ion Larmor diameter and that with this adjusted thickness the kinetic linear growth rate is in good agreement with that of MHD predictions. For the dusk side, the effective ion Larmor diameter is obtained from the ion Larmor diameter by the multiplicative factor  $(1 - 0.5 V_p/V_{thi})$  from equation 7 of Nakamura *et al.* [2010]; the effective ion Larmor diameter then equals the Larmor radius if  $V_p \sim V_{thi}$ . The Larmor radius of a 150-km/s proton in the magnetosheath (3.4 nT) is 450 km ( $0.18 R_M$ ).

[15] Miura and Pritchett [1982] used compressional ideal MHD to show that the wavelength  $\lambda$  of K-H waves at maximum linear growth scales as the thickness  $\Delta$  of the

velocity shear layer,  $\lambda \sim 2\pi \Delta$ . So for a 2800-km wavelength,  $\Delta$  is estimated to be 450 km, a value close to the estimated “effective” proton Larmor diameter, implying that kinetic theory is critical for the analysis of K-H waves at Mercury. The value of  $\Delta$  cannot be determined from magnetic field measurements, but a thickness of the current layer  $\Delta_C$  of 350 km ( $\Delta_C < \Delta$ ) can be estimated from the product of  $V_P$  and the transition time of  $\sim 2$  s across the magnetopause. Because of the lack of plasma flow measurements and the single-platform limitation, these estimates should be regarded as no more accurate than perhaps a factor of 2.

[16] For a value of  $M_S$  of 2.5, Miura [1992] gave the growth rate of the fastest-growing mode as  $0.04 \delta V/\Delta$ , from which the maximum growth rate is 0.04 radians/s. If the group velocity is  $\sim 110$  km/s, the wave would travel a distance of  $\sim 5 R_M$  from the nose of the magnetopause to the observation point in  $\sim 110$  s. Moreover, the  $e$ -folding would be  $\sim 4$ , suggesting that these waves could be in their nonlinear stage, as suggested by the highly steepened waves observed during M3 (Figure 3a). The transverse dimension can be estimated from the product of the spacecraft velocity and the duration of the encounter and is  $\sim 500$  km, less than the wavelength of 2800 km. Hasegawa et al. [2004, 2009] and Fairfield et al. [2007] demonstrated that sharply rolled-up K-H waves along the Earth’s magnetopause could be responsible for strong solar wind plasma transport into the Earth’s low-latitude boundary layer. M3 magnetic field observations imply that a similar mechanism could be important at Mercury.

[17] **Acknowledgments.** The MESSENGER project is supported by the NASA Discovery Program under contracts NAS5-97271 to the Johns Hopkins University Applied Physics Laboratory and NASW-00002 to the Carnegie Institution of Washington.

## References

- Anderson, B. J., M. H. Acuña, D. A. Lohr, J. Scheifele, A. Raval, H. Korth, and J. A. Slavin (2007), The Magnetometer instrument on MESSENGER, *Space Sci. Rev.*, *131*, 417–450, doi:10.1007/s11214-007-9246-7.
- Baker, D. N., et al. (2009), Space environment of Mercury at the time of the first MESSENGER flyby: Solar wind and interplanetary magnetic field modeling of upstream conditions, *J. Geophys. Res.*, *114*, A10101, doi:10.1029/2009JA014287.
- Berchem, J., and C. T. Russell (1982), The thickness of the magnetopause current layer: ISEE 1 and 2 observations, *J. Geophys. Res.*, *87*, 2108–2114, doi:10.1029/JA087iA04p02108.
- Chen, S.-H., and M. G. Kivelson (1993), On nonsinusoidal waves at the Earth’s magnetopause, *Geophys. Res. Lett.*, *20*, 2699–2702, doi:10.1029/93GL02622.
- Fairfield, D. H., A. Otto, T. Mukai, S. Kokubun, R. P. Lepping, J. T. Steinberg, A. J. Lazarus, and T. Yamamoto (2000), Geotail observations of the Kelvin-Helmholtz instability at the equatorial magnetotail boundary for parallel northward fields, *J. Geophys. Res.*, *105*, 21,159–21,173, doi:10.1029/1999JA000316.
- Fairfield, D. H., M. M. Kuznetsova, T. Mukai, T. Nagai, T. I. Gombosi, and A. J. Ridley (2007), Waves on the dusk flank boundary layer during very northward interplanetary magnetic field conditions: Observations and simulation, *J. Geophys. Res.*, *112*, A08206, doi:10.1029/2006JA012052.
- Hasegawa, H., M. Fujimoto, T.-D. Phan, H. Réme, A. Balogh, M. W. Dunlop, C. Hashimoto, and R. TanDorko (2004), Transport of solar wind into Earth’s magnetosphere through rolled-up Kelvin-Helmholtz vortices, *Nature*, *430*, 755–758, doi:10.1038/nature02799.
- Hasegawa, H., et al. (2009), Kelvin-Helmholtz waves at the Earth’s magnetopause: Multiscale development and associated reconnection, *J. Geophys. Res.*, *114*, A12207, doi:10.1029/2009JA014042.
- Lemaire, J. (1977), Impulsive penetration of filamentary plasma elements into the magnetospheres of Earth and Jupiter, *Planet. Space Sci.*, *25*, 887–890, doi:10.1016/0032-0633(77)90042-3.
- Masters, A., N. Achilleos, C. Bertucci, M. K. Dougherty, S. J. Kanani, C. S. Arridge, H. J. McAndrews, and A. J. Coates (2009), Surface waves on Saturn’s dawn flank magnetopause driven by the Kelvin-Helmholtz instability, *Planet. Space Sci.*, *57*, 1769–1778, doi:10.1016/j.pss.2009.02.010.
- Masters, A., et al. (2010), Cassini observations of a Kelvin-Helmholtz vortex in Saturn’s outer magnetosphere, *J. Geophys. Res.*, doi:10.1029/2010JA015351, in press.
- Miura, A. (1992), Kelvin-Helmholtz instability at the magnetospheric boundary dependence on the magnetosheath sonic Mach number, *J. Geophys. Res.*, *97*, 10,655–10,675, doi:10.1029/92JA00791.
- Miura, A. (1995), Dependence of the magnetopause Kelvin-Helmholtz instability on the orientation of the magnetosheath magnetic field, *Geophys. Res. Lett.*, *22*, 2993–2996, doi:10.1029/95GL02793.
- Miura, A., and P. L. Pritchett (1982), Nonlocal stability analysis of the MHD Kelvin-Helmholtz instability in a compressible plasma, *J. Geophys. Res.*, *87*, 7431–7444, doi:10.1029/JA087iA09p07431.
- Nakamura, T. K. M., H. Hasegawa, and I. Shinohara (2010), Kinetic effects on the Kelvin-Helmholtz instability in ion-to-MHD scale transverse velocity shear layers: Particle simulations, *Phys. Plasmas*, *17*, 042119, doi:10.1063/1.3385445.
- Odstroil, D., D. N. Baker, B. J. Anderson, L. R. Mayer, J. A. Slavin, and S. C. Solomon (2009), The space environment of Mercury at the time of the third MESSENGER flyby: Solar wind and IMF modeling of upstream conditions, *Eos Trans. AGU*, *90*(52), Fall Meet. Suppl., Abstract P24A-02.
- Otto, A., and D. H. Fairfield (2000), Kelvin-Helmholtz instability at the magnetotail boundary: MHD simulation and comparison with Geotail observations, *J. Geophys. Res.*, *105*, 21,175–21,190, doi:10.1029/1999JA000312.
- Owen, C. J., M. G. G. T. Taylor, I. C. Krauklis, A. N. Fazakerley, M. W. Dunlop, and J. M. Bosqued (2004), Cluster observations of surface waves on the dawn flank magnetopause, *Ann. Geophys.*, *22*, 971–983.
- Slavin, J. A., et al. (2008), Mercury’s magnetosphere after MESSENGER’s first flyby, *Science*, *321*, 85–89, doi:10.1126/science.1159040.
- Slavin, J. A., et al. (2009), MESSENGER observations of Mercury’s magnetosphere during northward IMF, *Geophys. Res. Lett.*, *36*, L02101, doi:10.1029/2008GL036158.
- Slavin, J. A., et al. (2010), MESSENGER observations of extreme loading and unloading of Mercury’s magnetic tail, *Science*, in press.
- Sonnerup, B. U. Ö., and M. Scheible (1998), Minimum and maximum variance analysis, in *Analysis Methods for Multi-Spacecraft Data*, *ISSI Sci. Rep. SR-001*, edited by G. Paschmann and P. W. Daly, pp. 185–220, Eur. Space Agency, Noordwijk, Netherlands.
- Spreiter, J. R., A. L. Summers, and A. Y. Alksne (1966), Hydromagnetic flow around the magnetosphere, *Planet. Space Sci.*, *14*, 223–253, doi:10.1016/0032-0633(66)90124-3.
- Wilber, M., and R. M. Winglee (1995), Dawn-dusk asymmetries in the low-latitude boundary layer arising from the Kelvin-Helmholtz instability: A particle simulation, *J. Geophys. Res.*, *100*, 1883–1898, doi:10.1029/94JA02488.
- B. J. Anderson and H. Korth, Johns Hopkins University Applied Physics Laboratory, 11100 Johns Hopkins Rd., Laurel, MD 20723, USA.
- L. G. Blomberg and T. Sundberg, Space and Plasma Physics, School of Electrical Engineering, Royal Institute of Technology, Teknikringen 31, SE-10044 Stockholm, Sweden.
- S. A. Boardsen and J. A. Slavin, Heliophysics Science Division, NASA Goddard Space Flight Center, Mail Stop 674, Greenbelt, MD 20771, USA. (scott.a.boardsen@nasa.gov)
- S. C. Solomon, Department of Terrestrial Magnetism, Carnegie Institution of Washington, 5241 Broad Branch Rd., NW, Washington, DC 20015, USA.